

# Flow visualization of the Newtonian and non-Newtonian behavior of fluids in a Tesla-diode valve

Shadi Ansari, Michael Bayans, Faezeh Rasimarzabadi and David S. Nobes\*

<sup>1</sup> University of Alberta, Department of Mechanical Engineering, Edmonton, Canada

\*david.nobes@ualberta.ca

## Abstract

A Tesla-diode valve allows restricted flow in one direction with the use of no moving parts and has many potential applications in different industrial situations. Understanding the flow through the valve is important for characterizing the performance of the device. In the present study, the effect of Newtonian and non-Newtonian nature of the fluid on the flow through a Tesla-diode valve is studied. Particle shadowgraph velocimetry (PSV) is used to visualize the velocity field. The results of this study showed that, as opposed to what is reported in the literature, a Newtonian fluid flow exiting from one stage of the valve, exhibits an unsteady behavior. The formation of vortices was observed, fluctuating in characteristics and moved toward the exit of the diode. The flow of the non-Newtonian fluid, however, showed stable flow within the Tesla-diode valve geometry at the same Reynolds number.

## 1 Introduction

The Tesla-diode valve (Tesla, 1920) is of interest as it has no moving parts but has the ability to have preferential flow in one direction. It has different applications in industry at both macro and micro scales based on its different advantages such as the ease of manufacturing, simplicity of operation, robustness, and low cost. It is not sensitive to contaminants, multiphase or oscillating flows. Some of the applications include: micro-pumps in MEMS devices to move small quantities of fluid (Nobakht, Shahsavan, & Paykani, 2013), electronics cooling at the chip scale (Scott M. Thompson, Jamal, Paudel, & Walters, 2013), and pulsating heat pipe to enhance its heat transfer capability (de Vries, Florea, Homburg, & Frijns, 2017).

The Tesla-diode valve has more resistance to flow in one direction compared to the reverse because of the particular arrangement of flow passages. The efficiency for flow control of a Tesla-diode valve can be expressed by the valve's diodicity and this can be used as an evaluation parameter for the performance of the design of the device. Diodicity is defined as the ratio of pressure drops for identical flowrates such that:

$$Di \equiv \left( \frac{\Delta P_{reverse}}{\Delta P_{forward}} \right) \quad (1)$$

A value with a diodicity that is greater than 1 indicates flow preference in the forward direction. The diodicity across a Tesla-diode valve with different configurations has been measured both numerically and experimentally (Lin, Zhao, Guest, Weihs, & Liu, 2015; T-Q & N-T Nguyen, 2003; S. M. Thompson, Paudel, Jamal, & Walters, 2014). In the forward direction, the pressure losses are similar to a simple duct flow. In the reverse direction, however, it is highlighted that the pressure loss is due to different phenomena in the flow such as a sudden expansion, flow splitting, and mini-jet impingement. It is reported that the geometry of a valve, valve-to-valve distance and number of valves in multistage design are important parameters in designing Tesla-diode systems.

Although almost all of the works report the effect of geometric properties of Tesla-diodes on the pressure loss, little information is found in the literature regarding the effect of flow and fluid properties. While parameters such as Reynolds number that describe the balance of forces are obvious design considerations, the effects of other flow and fluid properties on the general flow characteristics remain to be comprehensively understood. There appears to be no investigation into the effect of the working fluid, Newtonian vs. non-Newtonian, on flow structures and stability of the flow through the Tesla-diode valve.

Tesla-diode valves have the potential to be used as flow control devices in enhanced oil recovery methods such as steam assisted gravity drainage (SAGD)(Butler, 1998). The rheological properties of the produced oil may have an important influence on the performance of the Tesla-diode valve. The produced oil is typically a mixture of bitumen (4 -16 wt. %) and mineral solids (55-80 wt. %) in addition to water. This mixture has different rheological properties depending on its contents (Liu, Xu, & Masliyah, 2004). Pure bitumen behaves as a Newtonian fluid at low shear rates ( $\sim 10$  1/s). The presence of sand particles in the mixture, however, changes the Newtonian nature of the fluid to a non-Newtonian one having a shear-thinning behavior as reported in literature (Adeyinka, Samiei, Xu, & Masliyah, 2009). The amount of the mixed sand also has an effect on the non-Newtonian behavior of the fluid (Adeyinka et al., 2009). At low concentrations, where solid sands do not have strong interaction, their effect is negligible. At high concentrations, however, the interaction increases due to the decreased distance between particles of the suspended solids.

The non-Newtonian nature of a fluid can be modeled using the Ostwald-de Waele power law model (Schramm, 1994). This model describes the change in the viscosity of the fluid ( $\mu$ ) with respect to the applied shear rate ( $\gamma$ ) as a function of a flow consistency index ( $k$ ), and a flow index ( $n$ ) (Schramm, 1994) such that:

$$\mu = k * \gamma^{n-1} \quad (2)$$

In this paper, the effect of fluid rheology on the velocity distribution along a Tesla-diode valve is considered. The occurrence of flow fluctuation which has an effect on the performance of the diode is also covered for both Newtonian and non-Newtonian fluids. Particle shadow-graphic velocimetry (PSV) was used as the flow visualization techniques in the experiments. To achieve this, a multistage Tesla-diode based on Tesla's original patent (Tesla, 1920) was used. The primary use of the results will be to evaluate the potential application of the Tesla-diode in SAGD.

## 2 Experimental setup

A photograph of the optical setup used to perform PSV is shown in Figure 1(a). The setup includes a high speed camera (Phantom v611, Vision Research Inc.) coupled with a lens (Nikon AF NIKKOR 50mm f/1.8D lens), a high current LED, and a flow channel. The camera ran at 11,000 fps frame rate where the system was illuminated in a continuous mode using 4 in  $\times$  4 in LED. A flow channel to represent the multistage Tesla-diode geometry was designed as shown Figure 1 (b). This channel was made of two layers – a flow channel and a window for optical access. The flow channel was manufactured using a 3D printer (Form2, Formlabs Inc.) with a clear photoactive resin, allowing illumination in shadowgraph mode. Laser-cut acrylic sheet was the material used for the optical window covering the flow geometry. These two parts were then assembled and fastened using screws as shown in Figure 1 (c).

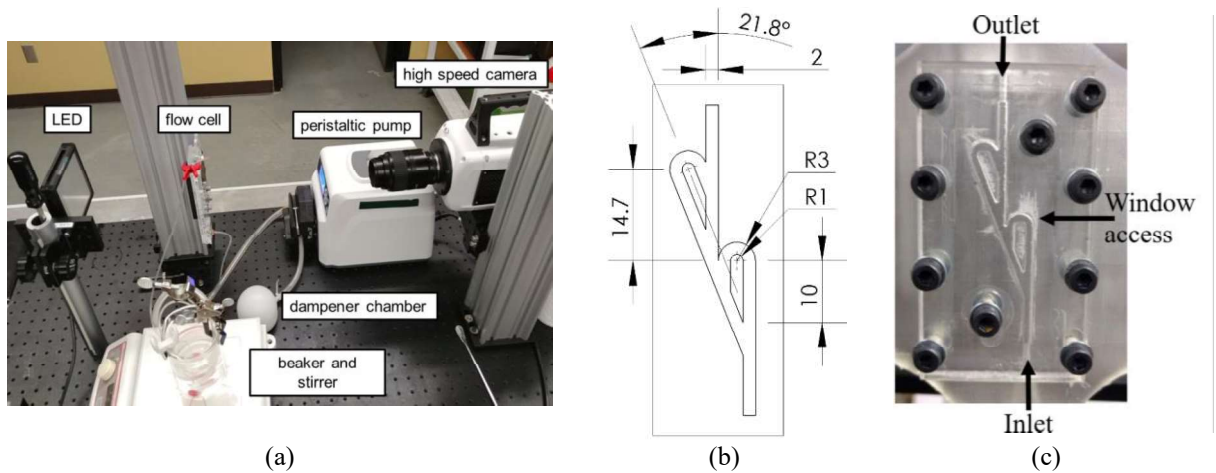


Figure 1 (a) picture of PSV test setup, (b) solid model and (c) picture of assembled flow channel

Water was the Newtonian fluid used for the experiments while a mixture of water and polyacrylamide was used as a non-Newtonian working fluid. A standard procedure was used to prepare 1000 ppm polyacrylamide solution (Ansari et al., 2015). This solution is a shear-thinning fluid with the flow consistency index of  $k = 0.054$  and flow index of  $n = 0.469$  (Ansari, 2016).

The experiments for both Newtonian and non-Newtonian fluids were performed at the same Reynolds number of 500. This was so that the effect of the rheology can be determined in the same flow regime. The viscosity of non-Newtonian fluids varies with respect to the shear rate which indicates that the traditional approach for the Reynolds number calculation is not applicable. The Reynolds number for non-Newtonian fluid is therefore calculated as (Kozicki, Chou, & Tiu, 1966):

$$Re^* = \frac{\rho D_h^n u^{2-n}}{k} \left( \frac{n}{a+bn} \right)^n 8^{1-n} \quad (3)$$

where  $\rho$  is the fluid density,  $D_h$  is the hydraulic diameter Tesla-diode valve entrance ;  $u$  is the average flow velocity; and  $a$  and  $b$  are constants depending on the shape of cross section of the channel. For square channels  $a = 0.2121$  and  $b = 0.6766$  (Kozicki et al., 1966). This relationship can also be used for Newtonian fluids by substituting  $k = \mu$  and  $n = 1$ . A peristaltic pump (Masterflex, Cole-Parmer) was used to provide the desired flow rate of the fluid through the diode. A dampening chamber was also used to remove flow fluctuations upstream to the inlet to the Tesla-diode valve. The fluid samples were seeded with  $40 \mu\text{m}$  tracer particles to capture the motion of the fluid.

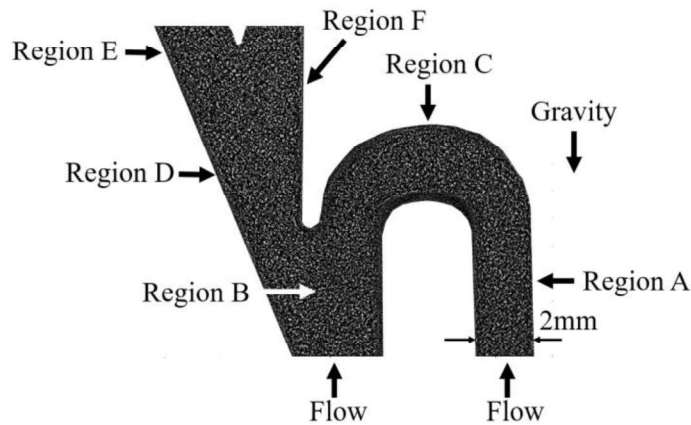


Figure 2. Raw image of water and  $40 \mu\text{m}$  tracer particle mixture using PSV

A sample of a pre-processed image of water flow captured using PSV is shown in Figure 2. The flow direction in this geometry was from bottom to top. The fluid is shown black and the tracer particles with  $40\ \mu\text{m}$  in diameter are shown as white dots. The flow channel is divided into six different regions to compare the phenomena happening in this geometry. The images captured by the PSV were then processed using a commercial software (DaVis 8.4, LaVision GmbH) to determine the velocity distribution.

### 3 Results

A comparison of the velocity distributions and the same Reynolds number for water and polyacrylamide are shown in Figure 3. The velocities at each condition were normalized based on the maximum velocity of the fluid in order to have a better comparison of the two cases. The velocity vector maps show that the fluids under these conditions followed different paths along the channels of the Tesla-diode valve. In both cases, the flows entered the Tesla-diode from Regions A and B. As shown in Figure 3 (a), for water, the incoming flow is dominated by flow in through Region A. This is because the majority of the flow entering this region has high inertia, forcing it to follow an initial straight path before entering the region having high curvature. Both fluid experiences their highest velocities in Regions C and D. The first increase in velocity which occurs in Region C is due to the presence of high curvature in the flow path. The increase in velocity in Region D however, is due to the presence of a convergence in the flow forming a *vena-contracta*. At this location, due to the presence of the sharp corners, the flow cannot follow the sudden change in the geometry. In this case the streamlines of the flow will converge and make a narrower jet with higher velocity at that location.

For polyacrylamide solution, shown in Figure 3 (b), the flow through Region B dominates. This fact is due to the non-Newtonian behavior of the fluid. Experimental studies on non-Newtonian flow showed that the shear-thinning behavior of fluids may delay the transition of a flow to turbulence which can be related to the drag-reduction properties of such fluids (Volokh, 2012). The *vena-contracta* effect was also observed in the non-Newtonian fluid where the maximum velocity occurs at Region D.

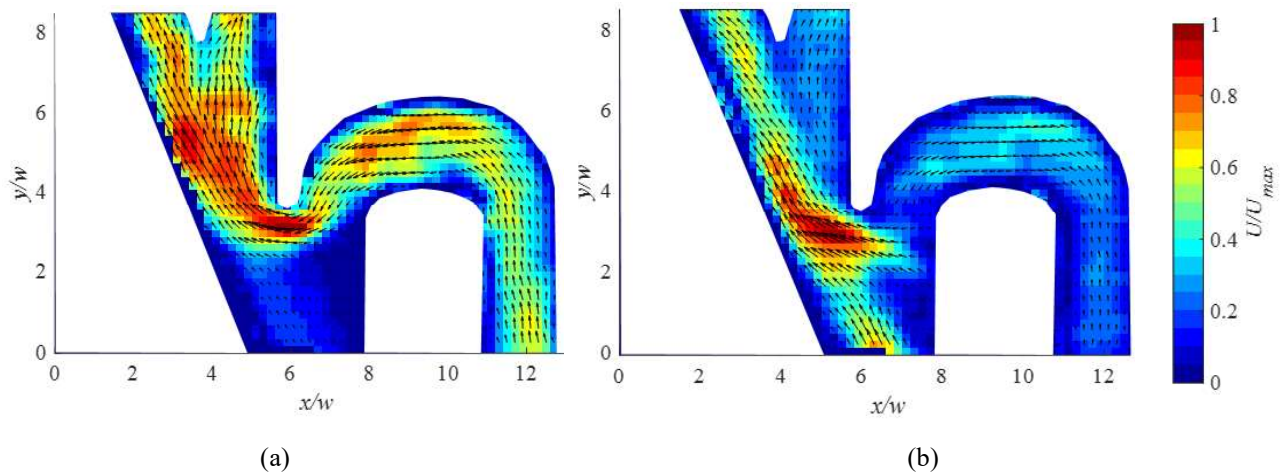


Figure 3. Normalized velocity vector map (a) water and (b) 1000 ppm polyacrylamide solution

A closer look at the velocity distribution within Region B, Figure 4(a), shows a location with minimum velocities for both water and polyacrylamide. Further investigation was therefore considered for this region. The velocity vector maps for both Newtonian and non-Newtonian flows in Region B are shown in Figure 4 (b) and (c). It can be seen that the flow for water cases had a coherent circulation occurs in this

region. The circulation for this flow occurred downstream ( $y/w = 1.5$ ) which is closer to the region with dominant inlet flow (Region C). In the flow of polyacrylamide, no circulation observed in this region.

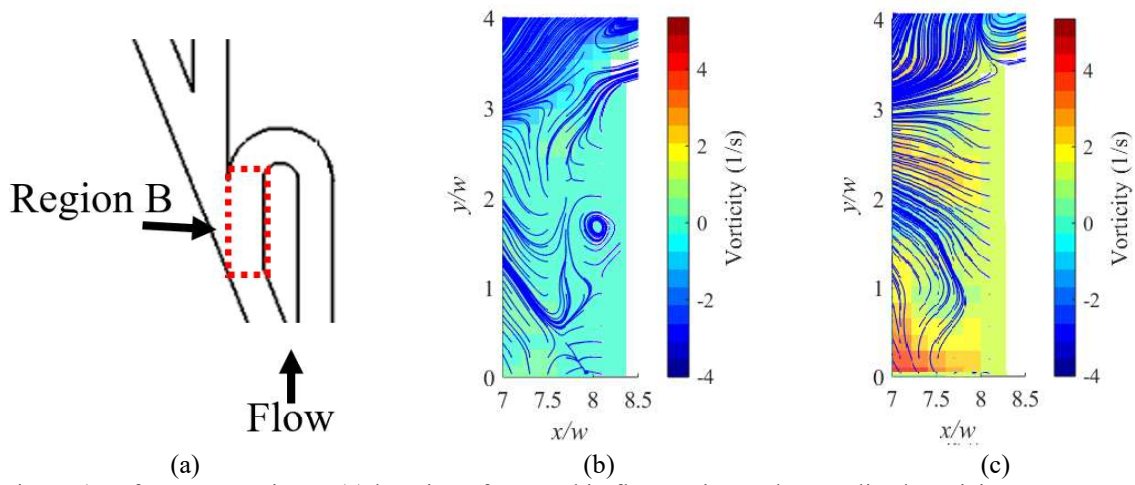


Figure 4. A focus on Region B:(a) location of zoomed in flow region and normalized vorticity vector map of (a) water and (b) 1000 ppm polyacrylamide solution

The effect of the fluid rheology on the flow was also indicated by differences in flow patterns at the exit of the first stage. For water, the flow was steady from the entrance of the valve up to Region D. Fluctuation in the flow was observed as the flow enters Region F. In this region, vortices started to form at locations that changed with time. Figure 5 (b) to (e) show the motion and the development of these vortices in the Tesla-diode valve in Region F. The streamlines of the flow at the  $t = t_0$  is shown in Figure 5 (b). In this time frame, the center of vortex was located at  $y/w = 6.5$ . At a later time ( $t = 2.3 \times 10^{-3}$  s), the center of the vortex moved closer to the entrance of the following valve at  $y/w = 7$ . As the vortex moves further downstream  $y/w = 7.5$  shown in Figure 5 (d), another vortex starts to form at  $y/w = 4.5$ . The generated vortex then moves closer to the entrance as shown in Figure 5 (e). The same cycle repeated over time. The presence of such a phenomenon results in the presence of an unsteady flow for the Newtonian fluid. In the non-Newtonian flow, however, a stable flow due to the delayed the transition to turbulence was observed.

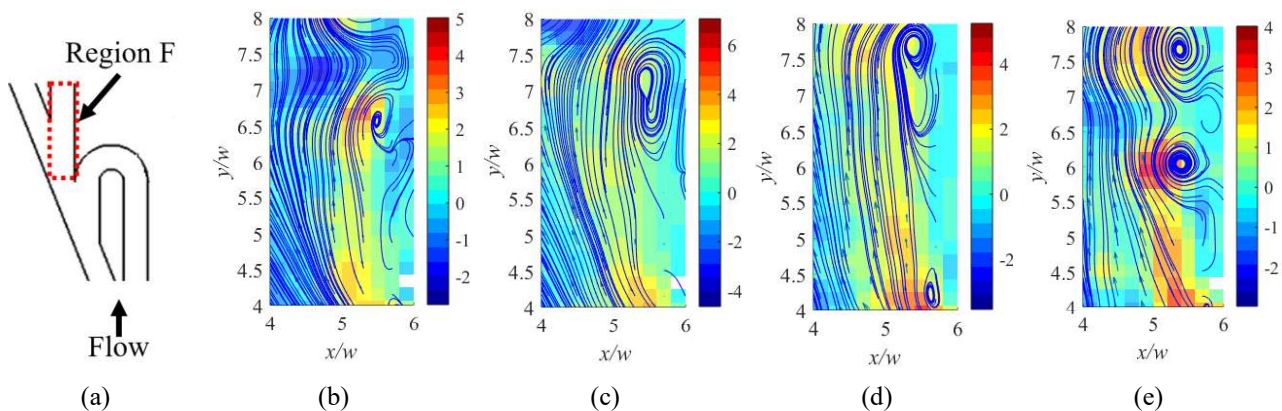


Figure 5. A focus on Region F with water flow: (a) location of zoomed in flow region, and streamlines of the flow motion with the vorticity at the background color map at (b)  $t = t_0$ , (c)  $t = t_0 + 2.3 \times 10^{-3}$  s (d)  $t = t_0 + 4.6 \times 10^{-3}$  s and (e)  $t = t_0 + 8.9 \times 10^{-3}$  s

## 4 Conclusion

The velocity distribution of a Newtonian and non-Newtonian fluid through a Tesla-diode valve at Reynolds number of 500 was studied using PSV. The results highlighted the importance of the fluid rheology on the performance and unique phenomena within the Tesla-diode valve. The results, in general, showed that there are significant differences between Newtonian and non-Newtonian flows that have to be accounted for when considering the application of Tesla-diode valves. The main variation in the flow pattern was seen through the different preferential flow at the inlet of the valve for water and polyacrylamide. The flow of Newtonian fluid showed an unsteady motion as the fluid exited one stage of the Tesla-diode valve. In case of non-Newtonian flow, the results indicated that the transition to turbulence was delayed which led to relatively more stable flow.

## Acknowledgements

The authors gratefully acknowledge financial support from Natural Sciences and Engineering Research Council (NSERC) of Canada, the Alberta Ingenuity Fund, and the Canadian Foundation for Innovation (CFI), and RGL Reservoir Management Inc.

## References

- Adeyinka, O. B., Samiei, S., Xu, Z., & Masliyah, J. H. (2009). Effect of particle size on the rheology of athabasca clay suspensions. *Canadian Journal of Chemical Engineering*, 87(3), 422–434.
- Ansari, S. (2016). *Newtonian and non-Newtonian flows through mini-channels and micro-scale orifices for sagd applications*. University of Alberta.
- Ansari, S., Rashid, A. I., Chatterjee, O., Waghmare, P. R., Ma, Y., & Nobes, D. (2015). Visualization of the viscous effects of non - Newtonian fluids flowing in mini - channels. *10th Pacific Symposium on Flow Visualization and Image Processing Naples*, 15–18.
- Butler, R. (1998). SAGD comes of age! *Journal of Canadian Petroleum Technology*, 37(7), 9–12.
- de Vries, S. F., Florea, D., Homburg, F. G. A., & Frijns, A. J. H. (2017). Design and operation of a Tesla-type valve for pulsating heat pipes. *International Journal of Heat and Mass Transfer*, 105, 1–11.
- Kozicki, W., Chou, C. H., & Tiu, C. (1966). Non-Newtonian flow in ducts of arbitrary cross-sectional shape. *Chemical Engineering Science*, 21(8), 665–679
- Lin, S., Zhao, L., Guest, J. K., Weihs, T. P., & Liu, Z. (2015). Topology Optimization of Fixed-Geometry Fluid Diodes. *Journal of Mechanical Design*, 137(8), 81402. <https://doi.org/10.1115/1.4030297>
- Liu, J., Xu, Z., & Masliyah, J. (2004). Role of fine clays in bitumen extraction from oil sands. *AIChE Journal*, 50(8), 1917–1927. <https://doi.org/10.1002/aic.10174>
- Nobakht, A. Y., Shahsavan, M., & Paykani, A. (2013). Numerical study of diodicity mechanism in different tesla-type microvalves. *Journal of Applied Research and Technology*, 11(6), 876–885.
- Schramm, G. (1994). A Practical Approach to Rheology and Rheometry. *Rheology*, 291.
- T-Q, T., & N-T Nguyen. (2003). Simulation and Optimization of Tesla Valves. *Optics Express*, 16, 14064
- Tesla, N. (1920). Valvular Conduit. 1,329,559, US Patent Off., App. Field,.
- Thompson, S. M., Jamal, T., Paudel, B. J., & Walters, D. K. (2013). Transitional and Turbulent Flow Modeling in a Tesla Valve. *Volume 7B: Fluids Engineering Systems and Technologies*,
- Thompson, S. M., Paudel, B. J., Jamal, T., & Walters, D. K. (2014). Numerical Investigation of Multistaged Tesla Valves. *Journal of Fluids Engineering*, 136(8), 81102.
- Volokh, K. Y. (2012). An investigation into the stability of a shear thinning fluid - arXiv, 1–14.